

Supporting Information

A self-calibrating dual responsive platform for sensitive detection of sulfite and sulfonic derivatives based on a robust Hf(IV) metal–organic framework

Kai Xing,^{ab} Ruiqing Fan,^{*a} Xiaoyuan Liu,^{bc} Shuang Gai,^a Wei Chen,^a Yulin Yang^{*a} and Jing Li^{*bc}

^a MIIT Key Laboratory of Critical Materials Technology for New Energy Conversion and Storage, School of Chemistry and Chemical Engineering, Harbin Institute of Technology, Harbin, 150001, P. R. China

^b Department of Chemistry and Chemical Biology, Rutgers University, 123 Bevier Road, Piscataway, New Jersey, 08854, United States

^c Hoffmann Institute of Advanced Materials, Shenzhen Polytechnic, 7098 Liuxian Blvd, Nanshan District, Shenzhen, 518055, P.R. China

Contents

Section 1. Materials and Methods.....	3
Section 2. Synthesis of Hf-PBTA	5
Section 3. Structural Simulations.....	7
Section 4. PXRD Patterns of Hf-PBTA	8
Section 5. Thermogravimetric Analysis for Hf-PBTA	10
Section 6. Photoluminescence Measurements	11
References	29

Section 1. Materials and Methods

Chemicals and Instruments

All reagents were commercially available and used without further purification. Powder X-ray diffraction (PXRD) patterns were recorded in a 2θ range of 3° – 40° with a scan speed of $2^{\circ} \text{ min}^{-1}$ using $\text{Cu K}\alpha$ ($\lambda = 1.5406 \text{ \AA}$) radiation by Rigaku Ultima-IV X-ray Diffractometer. The thermal analysis was performed on the TA Instruments Q5000 analyzer with flow thermogravimetric analyzer from room temperature to 700°C with heating rate of $10^{\circ}\text{C min}^{-1}$ under a flow of nitrogen. UV-vis spectra were obtained on Shimadzu UV-3600 spectrophotometer in the range of 200–800 nm at room temperature. The fluorescence spectra were recorded on a fluorescence and absorbance spectrometer, Duetta, Horiba Scientific at 298 K. Scan electron microscope (SEM) images were recorded by Rili SU 8000HSD Series Hitachi New Generation Cold Field Emission SEM.

Chemical stability test

10 mg finely ground Hf-PBTA powders was immersed in 5 mL of solution with different pH values for 48 h; then the MOF powders were centrifuged and used to measure the PXRD patterns.

Fluorescence Measurement and Titration

For the fluorescence measurements, a typical experimental procedure was set up. Crystalline samples of Hf-PBTA (3 mg) were finely ground and added to a vial containing deionized water (3 mL), followed by ultrasonication treatment for 30 min, forming a suspension solution. The aqueous solution (1 mM) of analyte was added to the above suspension solution to form the analytes incorporated MOF suspension for the fluorescence studies.

To have access to the relationship between response efficiency of Hf-PBTA and concentration of analytes, the fluorescent emissions of Hf-PBTA suspension solutions were carried out by incrementally adding freshly prepared aqueous solutions of analytes (1 mM) to the sensor suspension under steady stirring (10 μ L addition each time).

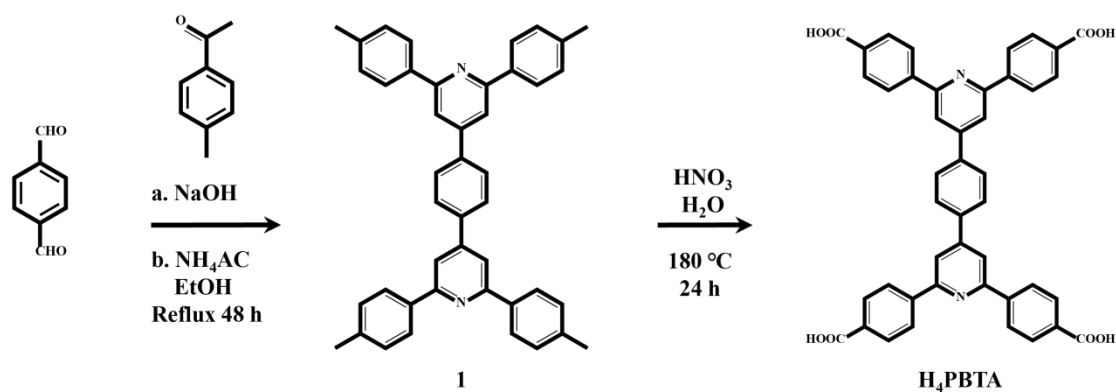
Computational Methods

The geometries of H₄PBTA without and with sulfite cations were performed with Gaussian09 program. To the ground state, the density functional theory (DFT) were applied using range-separated CAM-B3LYP functional together with 6-31g+(d,p) basis set in the conductor-like polarizable continuum model (CPCM) after considering the solvent effects of water ($\epsilon = 78.36$). Accordingly, the geometries of excited states were optimized using the time-dependent density functional theory (TDDFT) with CAM-B3LYP functional and 6-31g+(d,p) basis set.

Section 2. Synthesis of Hf-PBTA

S2A. Synthesis of 4,4',4'',4'''-(1,4-phenylenebis(pyridine-4,2,6-triyl))tetrabenzoic acid (H₄PBTA)

The synthesis of H₄PBTA was carried out according to reported procedure.



Scheme S1. Synthesis of H₄PBTA ligand.

1,4-Bis(2,6-di-p-tolylpyridin-4-yl)benzene (1). 4-Methylacetophenone (5.60 mL, 42 mmol), terephthalaldehyde (1.30 g, 10.0 mmol) and NaOH (2.40 g, 60 mmol) were combined and crushed together with a pestle and mortar for 1 h manually to make the two reactants react sufficiently. The resultant solid was dissolved in EtOH (200 mL) with NH₄OAc (15 g, excess) and the solution heated under reflux for 48 h. On cooling to the temperature, a precipitate was filtered, washed with water three times and dried in an 80 °C oven to afford the rough product, which was recrystallized with toluene to yield light yellow crystals (2.57 g, 43 %). ¹HNMR (CDCl₃, 400 MHz, ppm) δ: 8.12 (d, 8H), 7.90 (s, 8H), 7.33 (d, 8H) 2.45 (s, 12H).

4,4',4'',4'''-(1,4-phenylenebis(pyridine-4,2,6-triyl))tetrabenzoic acid (H₄PBTA). The light yellow crystals (2.0 g) were combined with concentrated HNO₃ (3.00 mL) and distilled water (36 mL) in an autoclave and heated at 180 °C for 24 h. The reaction was cooled to room temperature and the solid was collected and washed with distilled

water and acetone for three times, respectively. The obtained orange solid was dried under at an 80 °C oven (1.64 g, 68.3 %). ¹H NMR (DMSO-*d*₆): 13.13 (s, 4H), 8.52 (d, 8H), 8.47 (s, 4H), 8.32 (s, 4H), 8.14 (d, 8H).

S2B. Synthesis of Hf-PBTA.

HfOCl₂ (43 mg, 0.10 mmol) and acetic acid (1.5 mL) were mixed in 5 mL of DMF in a 10 mL Pyrex vial and dissolved using sonication. The clear solution was incubated in an oven at 80 °C for 1h. After cooling down to room temperature, H₄PBTA (24 mg, 0.035 mmol) was added to this solution and the resulting mixture was sonicated for 10 min. The vial was then heated in an oven at 120 °C for 48 h. After cooling to room temperature, the resulting yellow crystals were harvested by filtration and washed with DMF and acetone, and then dried in air (yield 32 mg).

Section 3. Structural Simulations

The Crystal Builder and Forcite modules of Materials Studio 7.0 software¹ were used to construct preliminary crystallographic structures of the hypothetical metal-organic frameworks. As shown in Fig. S1, the PXRD pattern of Hf-PBTA matches well with that of the BUT-15 (Zr), indicating that the formation of Hf-PBTA is isorecticular to BUT-15 (Zr) and their structural topologies and clusters are identical. Hence, we combined (Hf₆O₄(OH)₈(H₂O)₄) clusters with the H₄PBTA linkers into a preliminary MOF structure by using the BUT-15 as a templating structure.

The optimization of the preliminary structures using the Forcite module was based on the Universal force field,² which was used to describe the bonded and the short-range non-bonded. The optimization was itself done in two steps. In the first step, the structure was optimized under the constraint of fixed unit cell parameters to release some strain by allowing the building blocks to accommodate in a more energetically favorable position. The new structures were used as input for the second step, where they were optimized only under the constraint of fixed unit cell angles. Then, Rietveld refinements was applied to define the lattice parameters, producing the refined PXRD profile with the lattice parameters of $a = b = 20.598 (\pm 0.012) \text{ \AA}$ and $c = 66.729 (\pm 0.047) \text{ \AA}$. The wR_p and R_p values converged to 5.80 % and 3.84 %, respectively (line broadening from the crystallite size and lattice strain were both concerned). Similar method has been successfully adopted by other groups.³⁻⁶

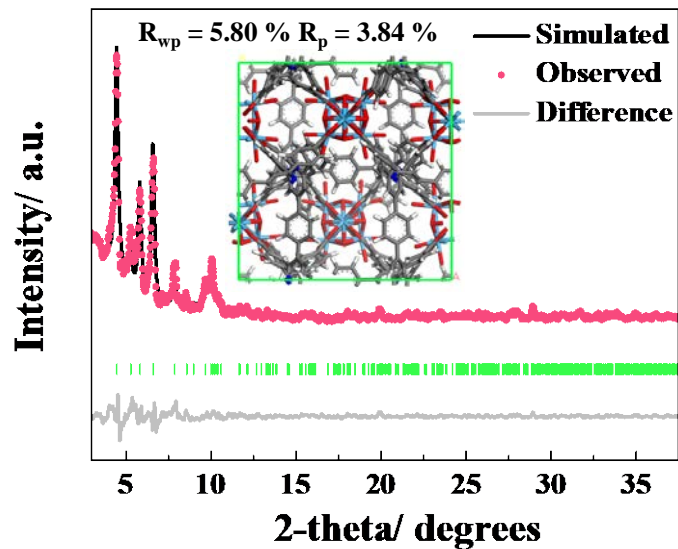


Fig. S1 Rietveld refinement of X-ray diffraction patterns of Hf-PBTA (The Bragg positions are marked as green bars).

Section 4. PXRD Patterns of Hf-PBTA

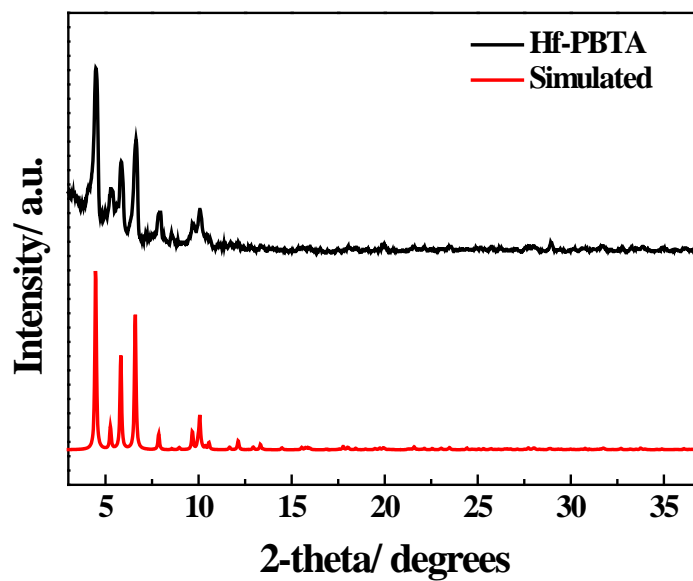


Fig. S2 PXRD patterns of as synthesized Hf-PBTA and the simulated BUT-15 (Zr).

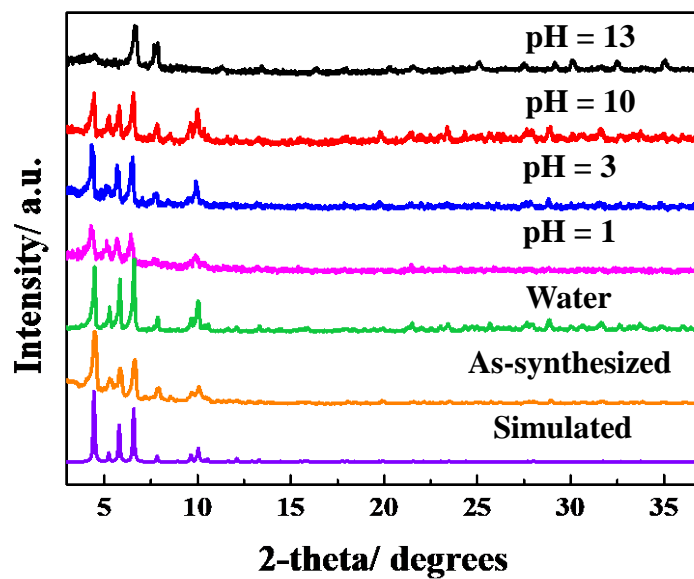


Fig. S3 PXRD patterns of Hf-PBTA after treatment in water and aqueous solution with different pH.

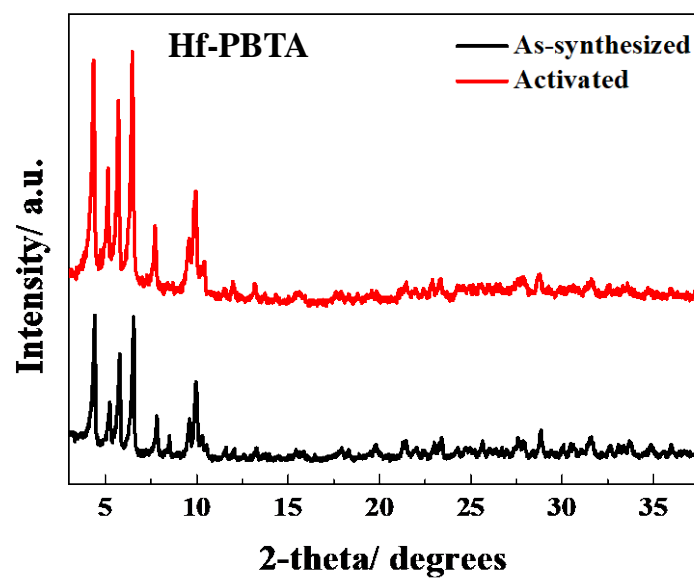


Fig. S4 PXRD patterns of Hf-PBTA before and after activation.

Section 5. Thermogravimetric Analysis for Hf-PBTA

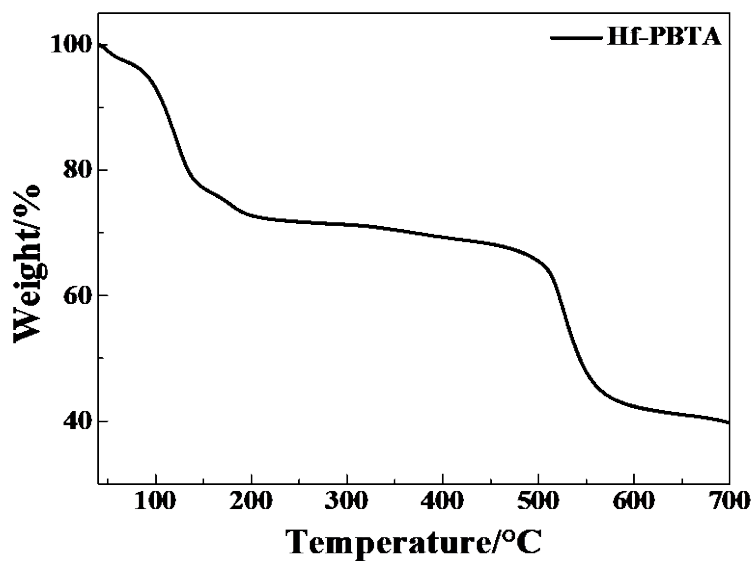


Fig. S5 TGA curve of Hf-PBTA.

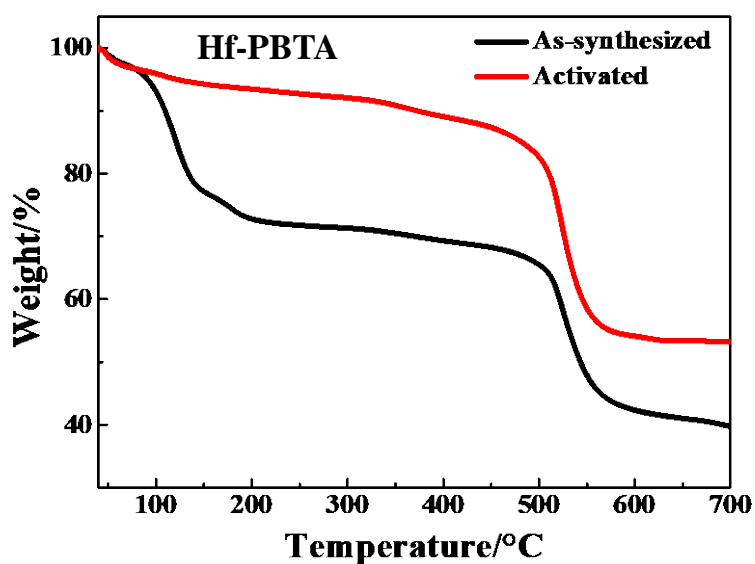


Fig. S6 TGA curves of the as-synthesized Hf-PBTA and the sample after activation.

Section 6. Photoluminescence Measurements

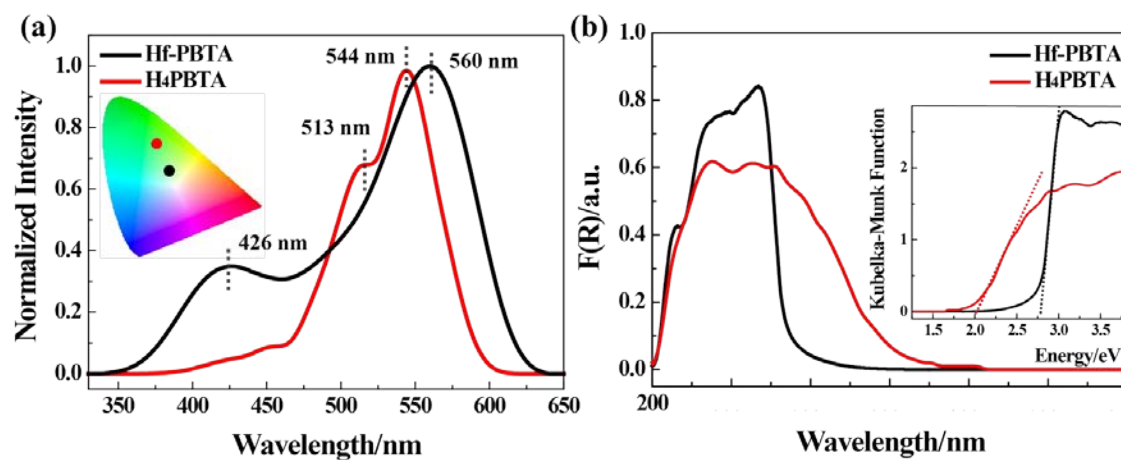


Fig. S7 (a) Fluorescence emission spectra of **Hf-PBTA** and ligand in the solid state and at room temperature ($E_x = 320$ nm); (b) Solid UV-Vis spectra of **Hf-PBTA** and ligand.

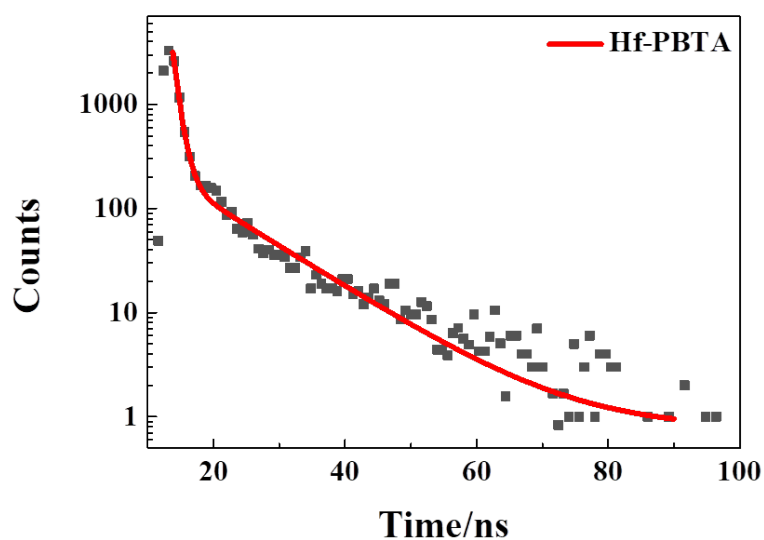


Fig. S8 The lifetime of **Hf-PBTA** in solid state at 298K.

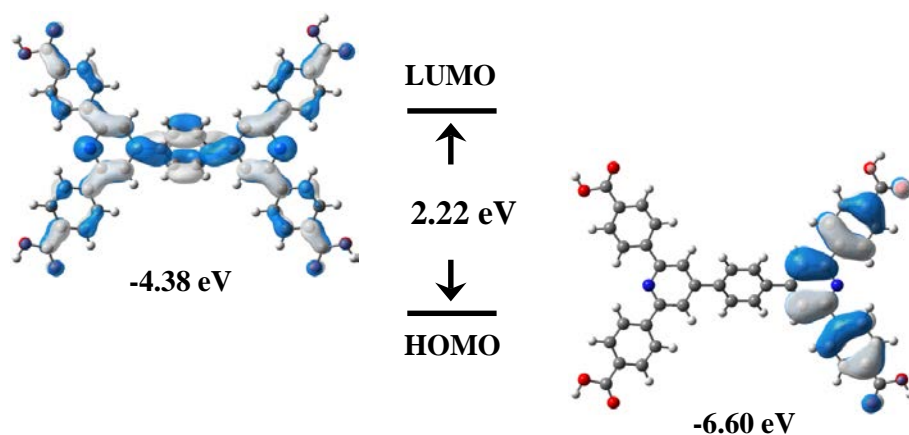


Fig. S9 Calculated HOMO and LUMO orbitals of **Hf-PBTA** and the HMO-LUMO energy gap, plotted with an isovalue of 0.04.

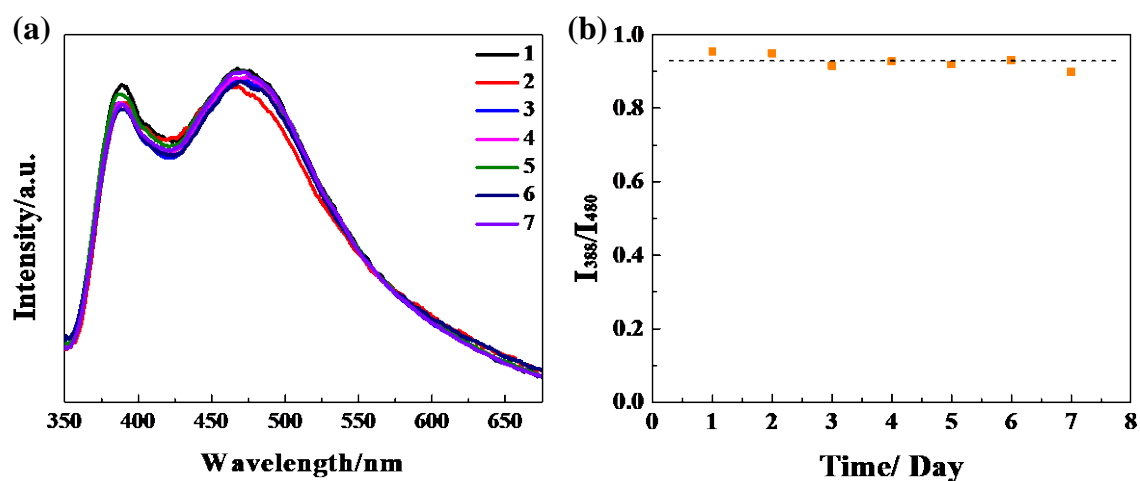
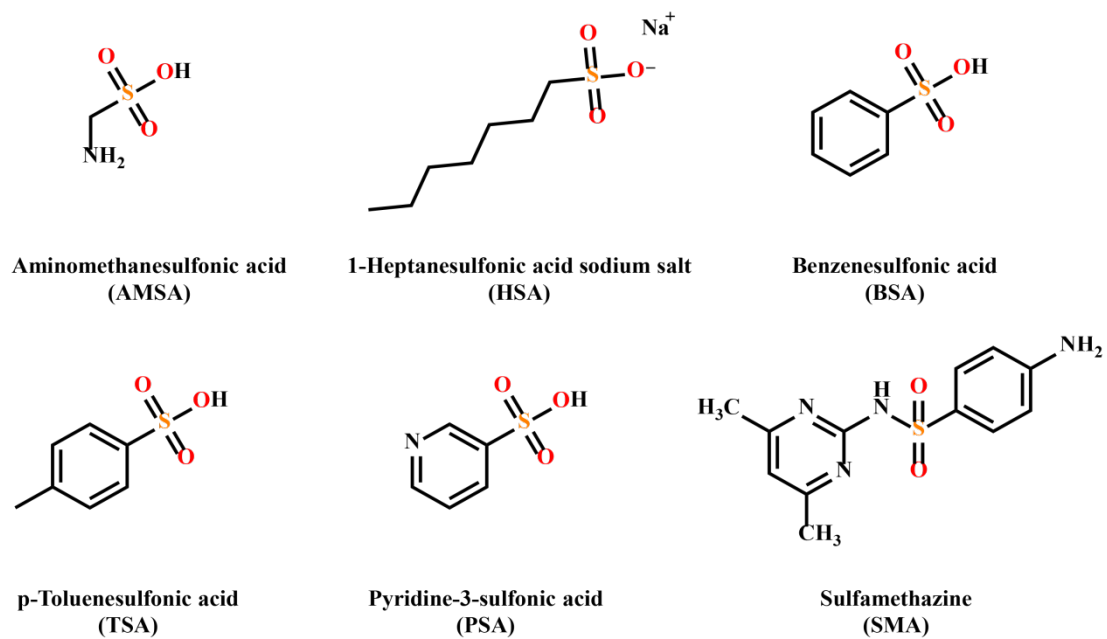


Fig. S10 (a) Fluorescence emission spectra of **Hf-PBTA** in the aqueous solution at room temperature for one week (Ex = 330 nm); (b) The intensity ratio of **Hf-PBTA** in the aqueous solution at room temperature for one week.



Scheme S2. Structures of the selected sulfonic analytes.

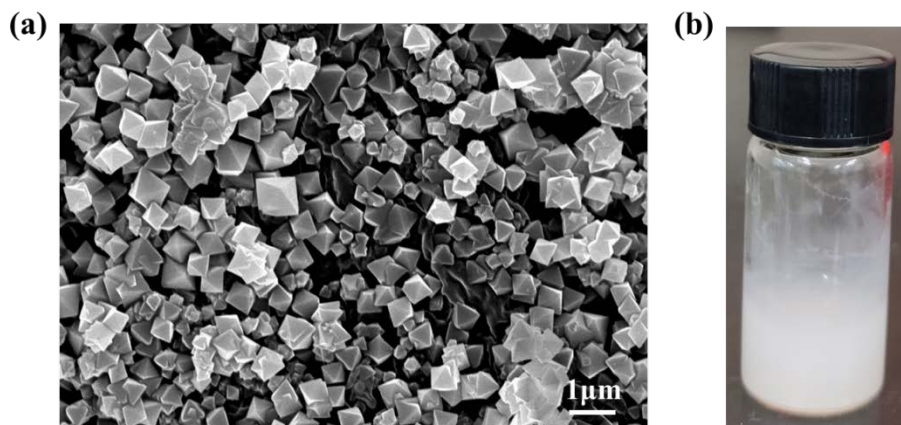


Fig. S11 (a) SEM image of Hf-PBTA; (b) Photograph of Hf-PBTA solution after 4 hours.

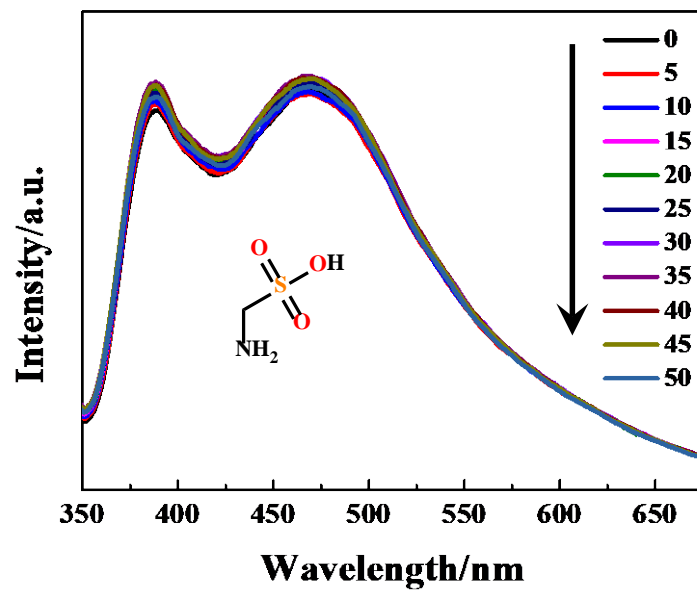


Fig. S12 Fluorescence spectra of Hf-PBTA in the presence of AMSA in water (Ex = 330 nm).

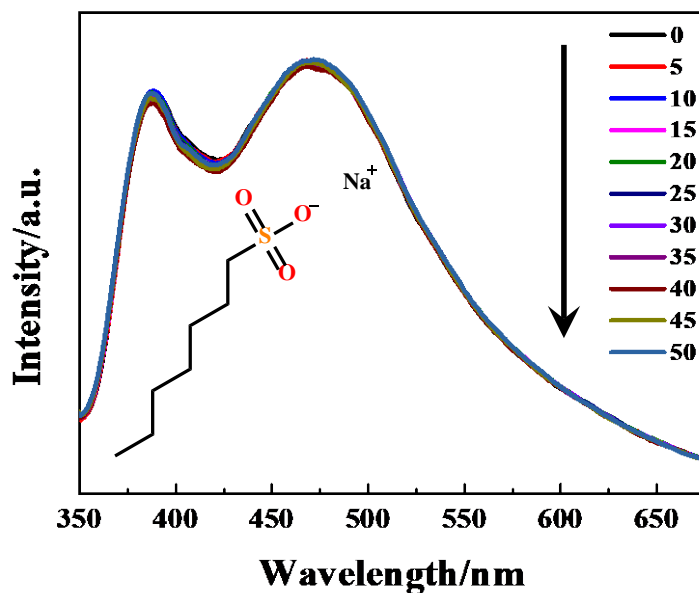


Fig. S13 Fluorescent spectra of Hf-PBTA in presence of HSA in water (Ex = 330 nm).

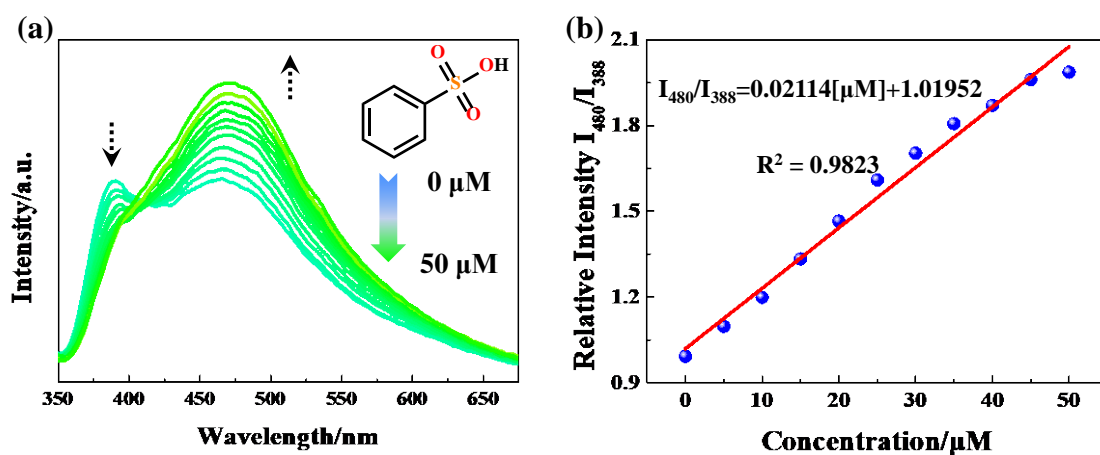


Fig. S14 (a) Effect on the fluorescence of Hf-PBTA dispersed in water upon the incremental addition of BSA (Ex = 330 nm); (b) linear fit for the estimation of detection limit.

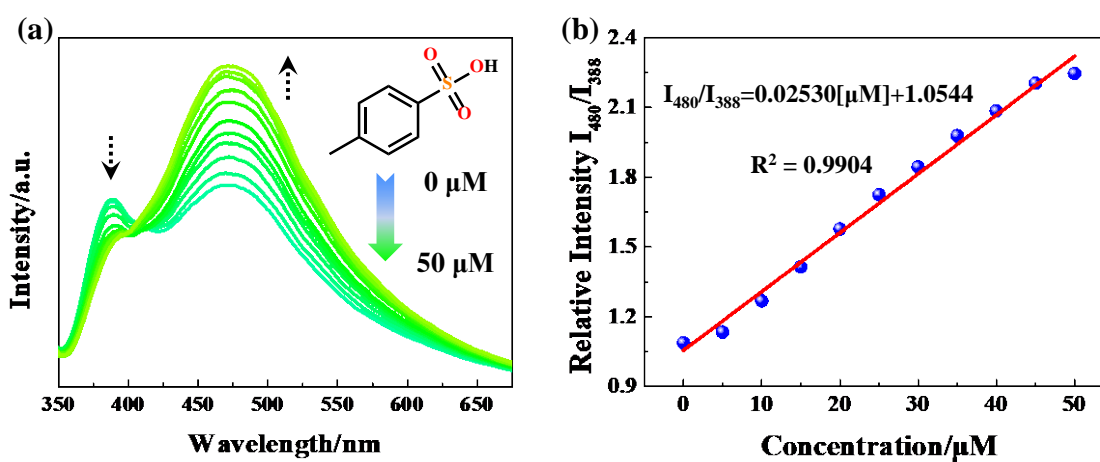


Fig. S15 (a) Effect on the fluorescent spectra of Hf-PBTA dispersed in water upon the incremental addition of TSA (Ex = 330 nm); (b) linear fit for the estimation of detection limit.

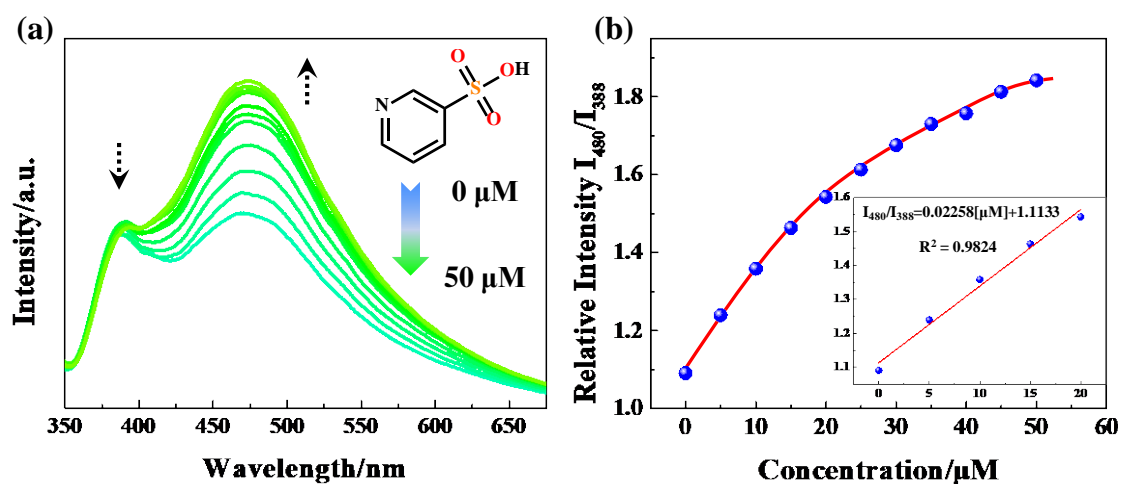


Fig. S16 (a) Effect on the fluorescence of Hf-PBTA dispersed in water upon the incremental addition of PSA (Ex = 330 nm); (b) linear fit for the estimation of detection limit.

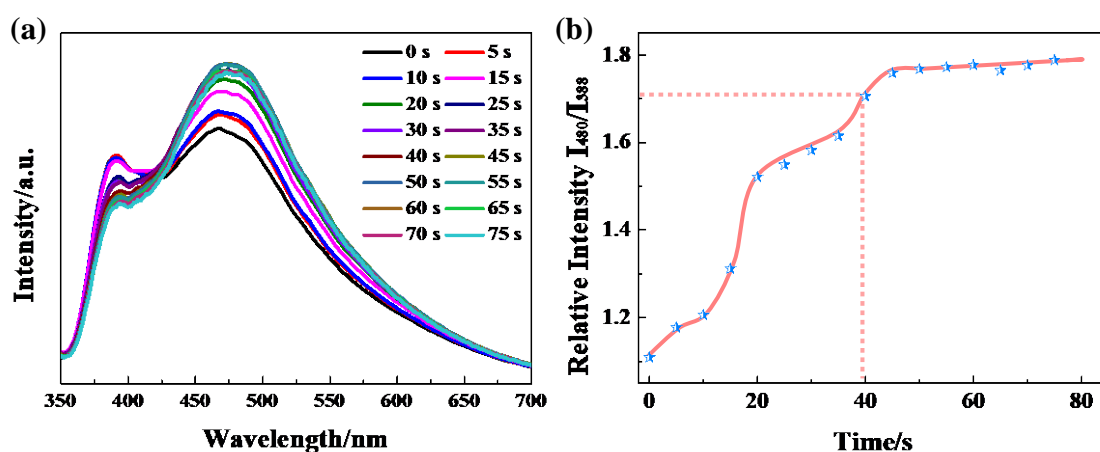


Fig. S17 Response time of Hf-PBTA towards BSA (a) and its variation of intensity ratio (b) (Ex = 330 nm).

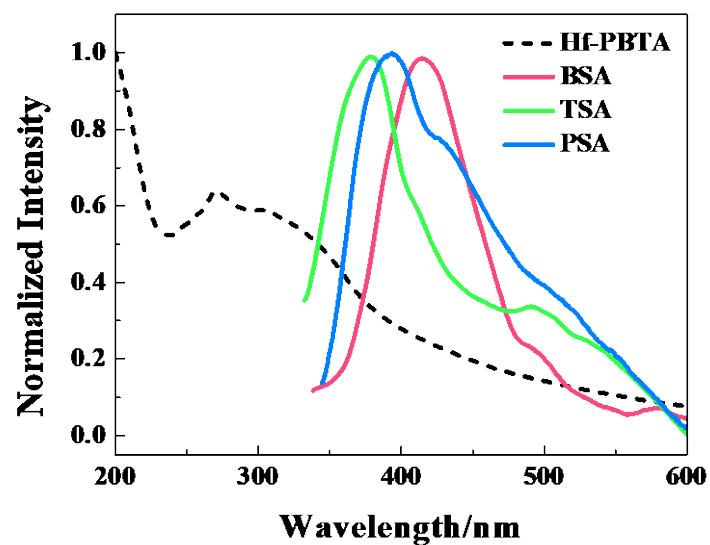


Fig. S18 Emission spectra of aromatic sulfonic analytes (solid lines) and UV absorbance of Hf-PBTA (dashed line).

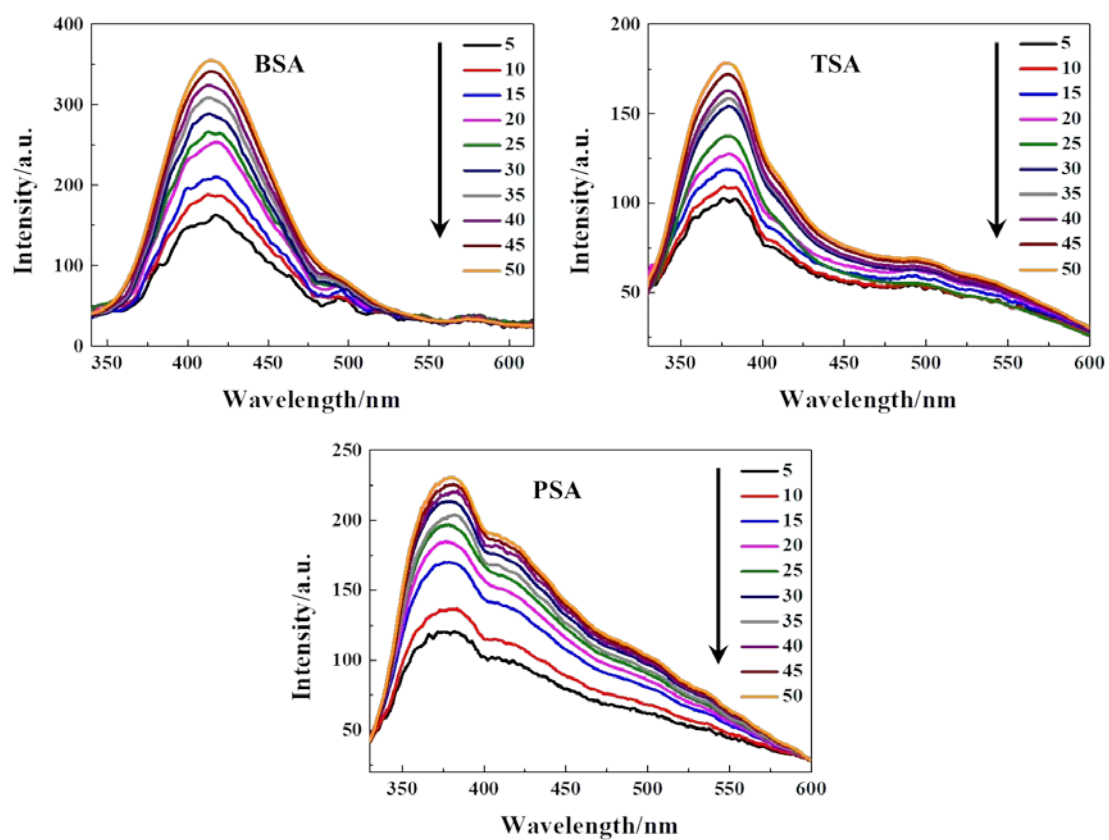


Fig. S19 The emission of BSA, TSA and PSA in the 5-50 μ M.

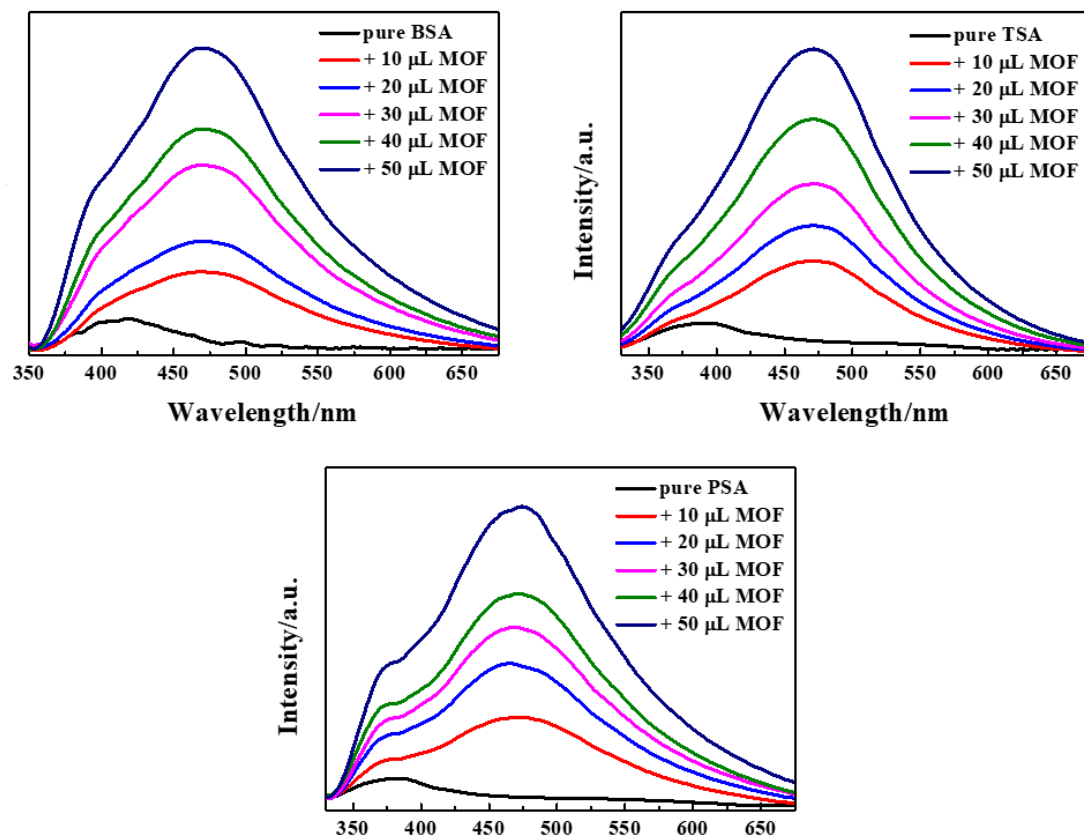


Fig. S20 The emission of saturated BSA, TSA and PSA solutions with addition of Hf-PBTA suspension.

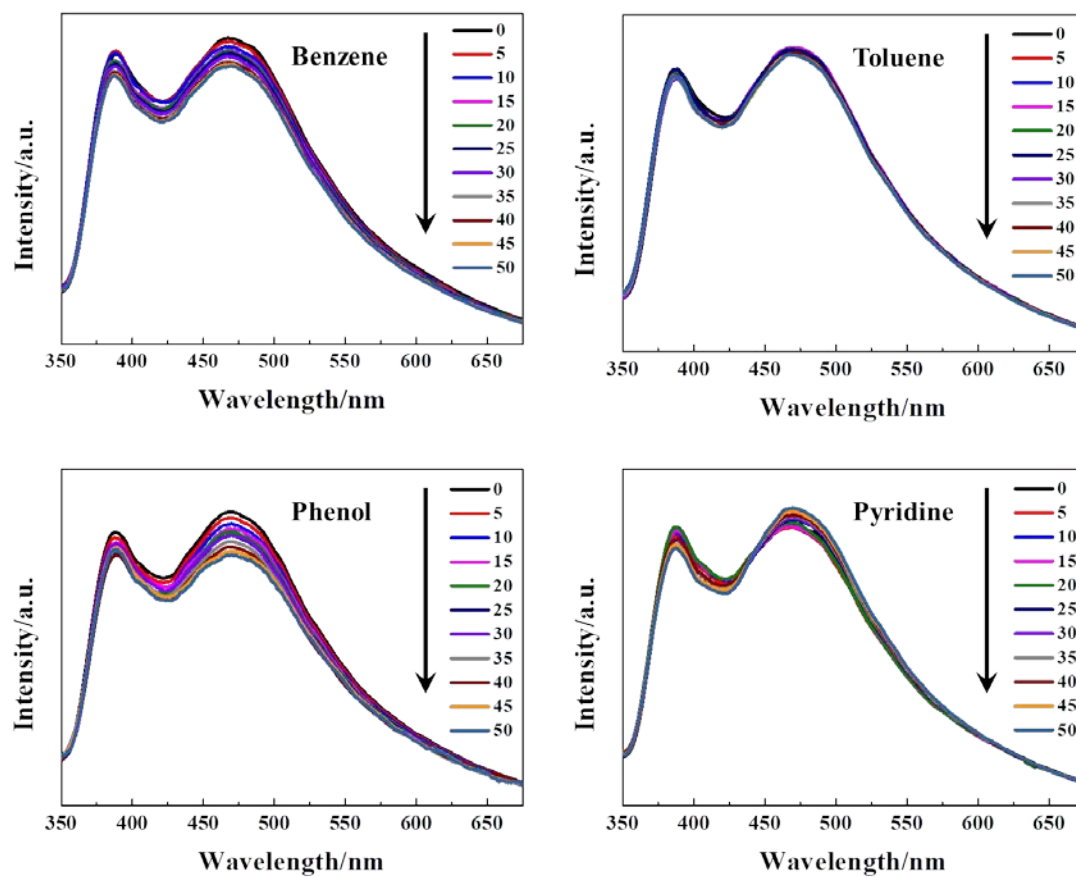


Fig. S21 Effect on the fluorescence of **Hf-PBTA** dispersed in water upon the incremental addition of benzene, toluene, phenol and pyridine (Ex = 330 nm).

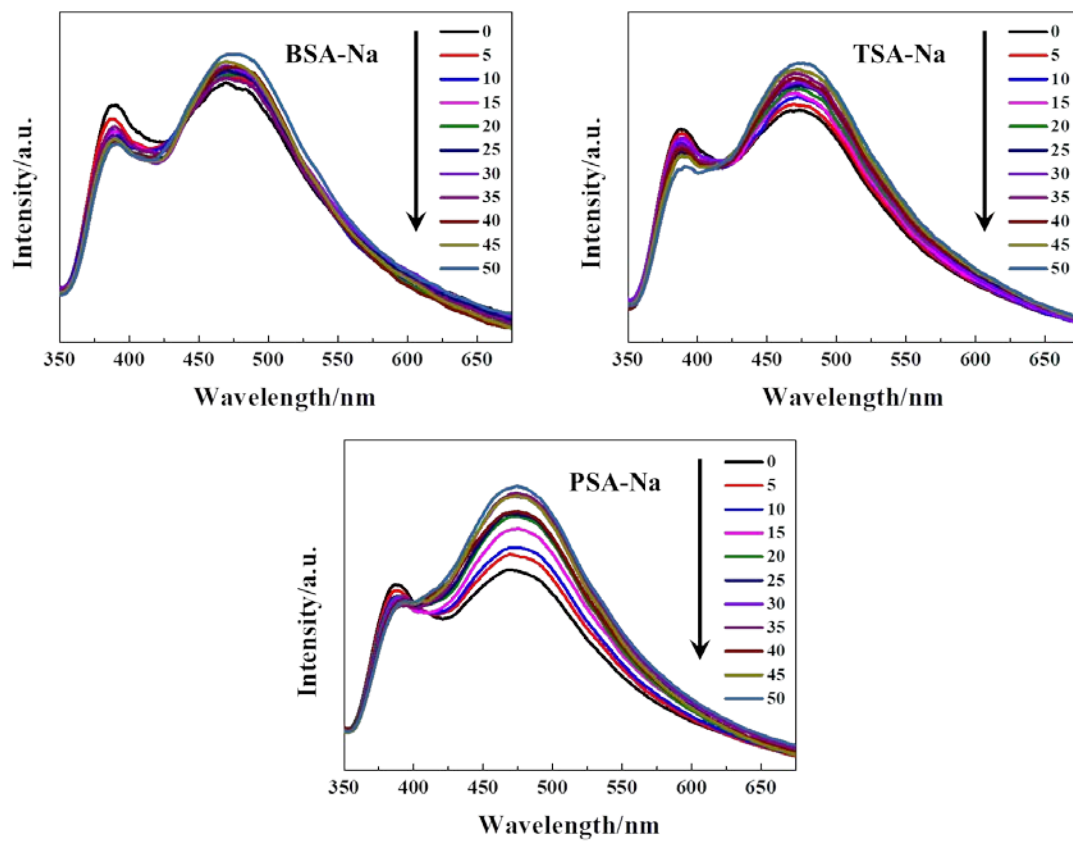


Fig. S22 Effect on the fluorescence of **Hf-PBTA** dispersed in water upon the incremental addition of BSA-Na, TSA-Na, and PSA-Na (Ex = 330 nm).

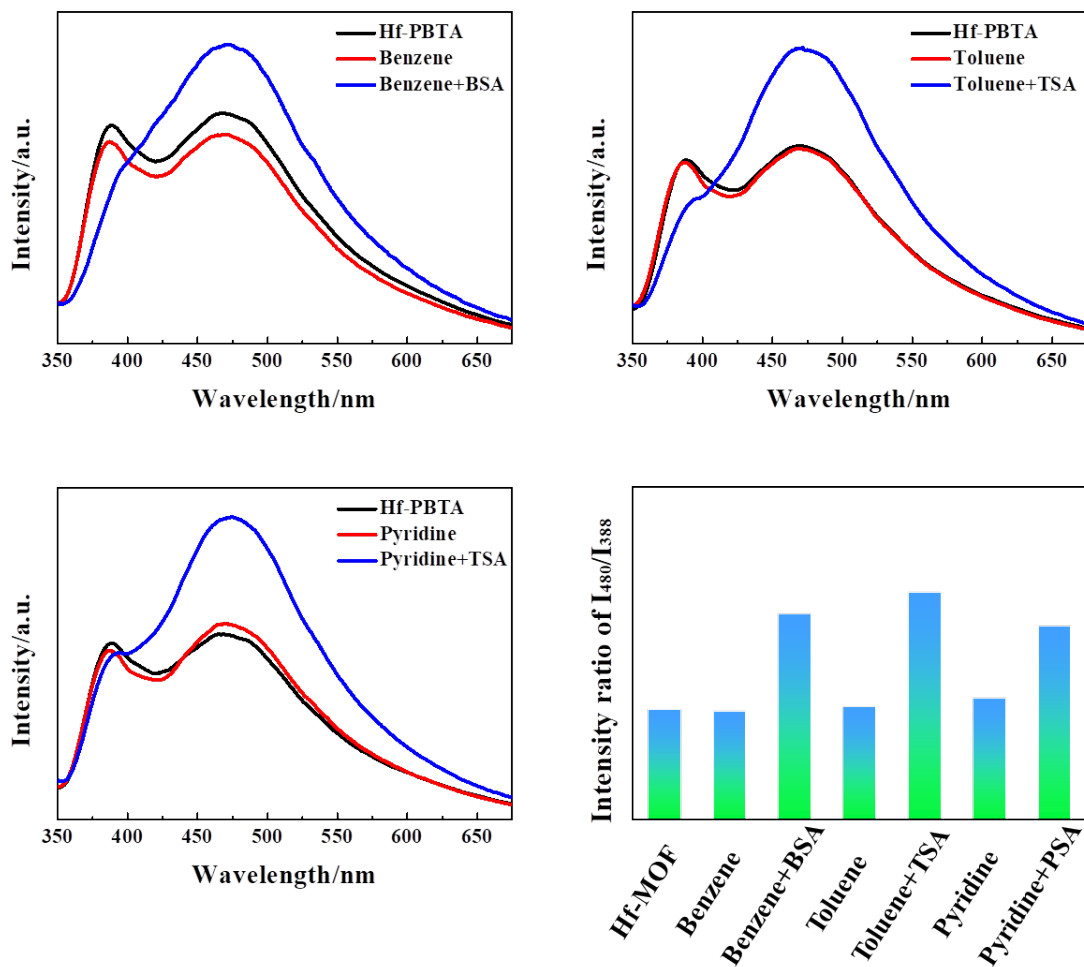


Fig. S23 Competition experiments: Fluorescence spectra of **Hf-PBTA** before and after adding aromatic molecules without and with sulfonic acid group to the above solution (Ex = 330 nm).

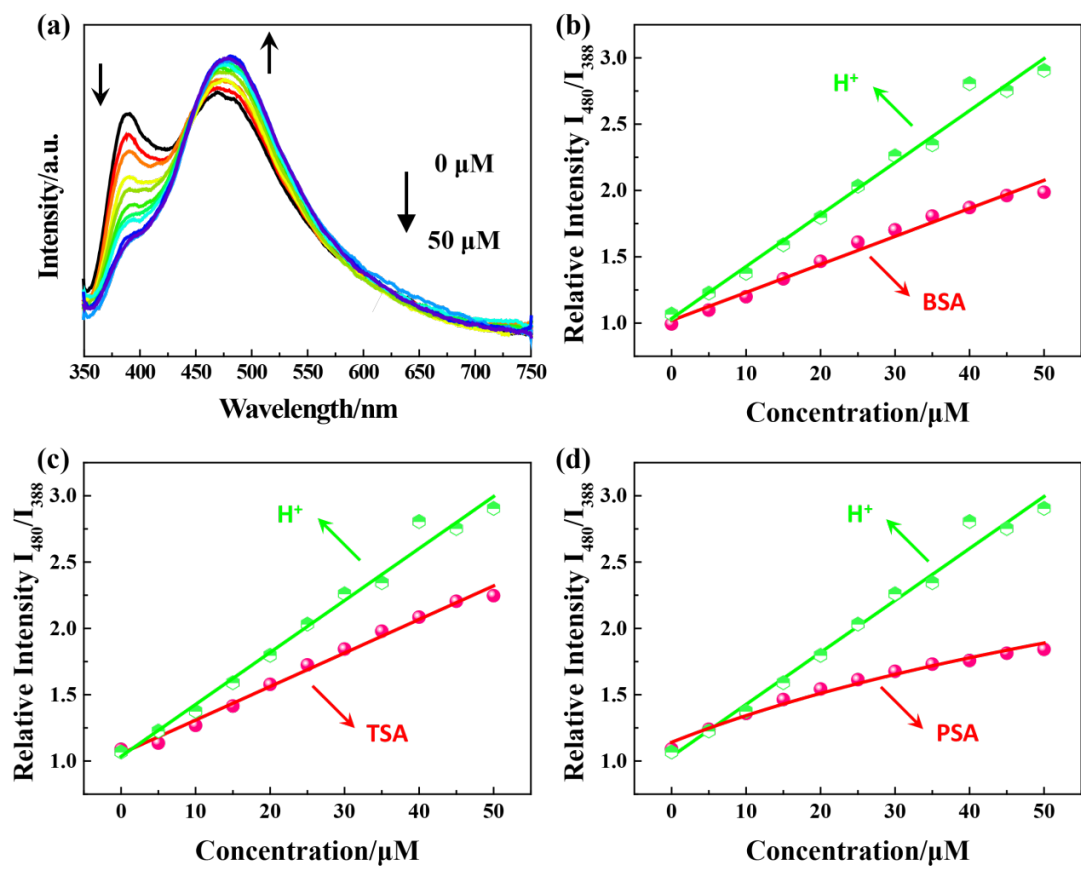


Fig. S24 (a) Effect on the fluorescence of **Hf-PBTA** dispersed in water upon the incremental addition of HCl (pH = 3.0) (Ex = 330 nm). The quantitative contribution of pH to sensing signal at the same concentration as BSA (b), TSA (c) and PSA (d).

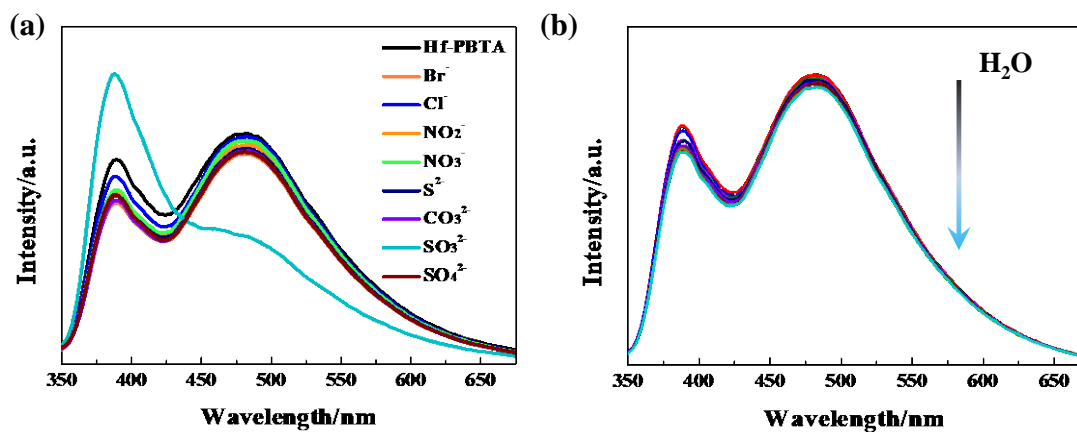


Fig. S25 (a) Fluorescent response of **Hf-PBTA** to different anions in the same concentration of $50 \mu\text{M}$ at room temperature ($\text{Ex} = 330 \text{ nm}$); (b) Influence of water on fluorescence of **Hf-PBTA**.

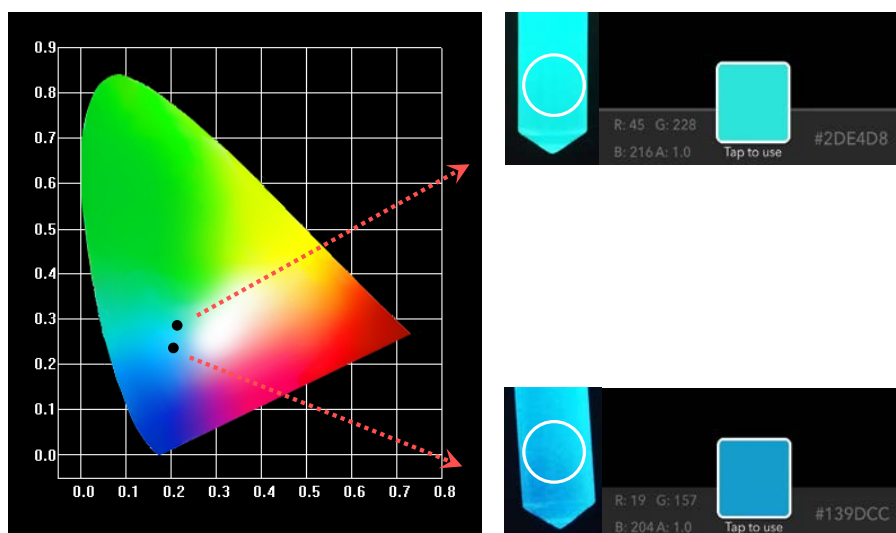


Fig. S26 The Commission Internationale d'Eclairage (CIE) coordinate before and after addition of $50 \mu\text{M}$ Na_2SO_3 and its fluorescence color images. The G/B ratio was recorded by color-scanning application in the smartphone.

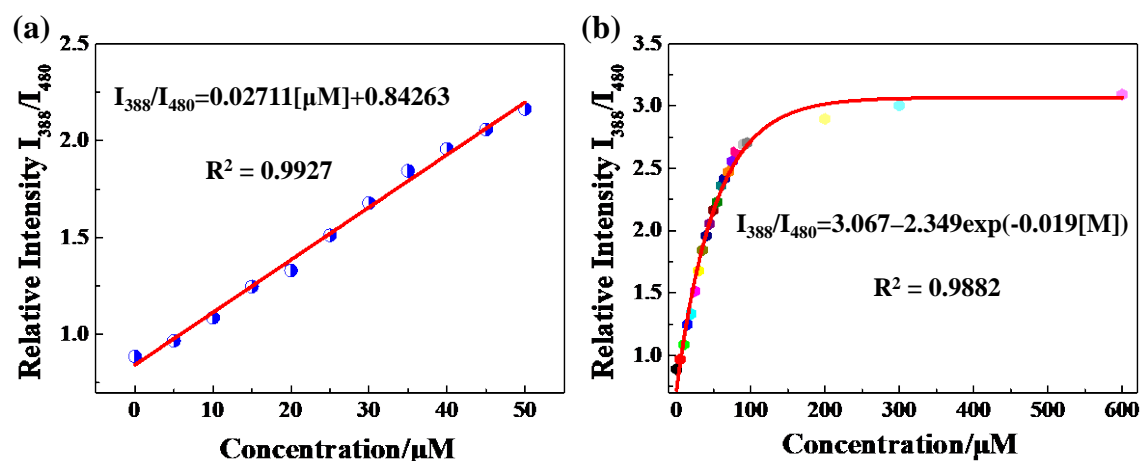


Fig. S27 Concentration dependence of the fluorescence intensity ratio (I_{388}/I_{480}) in the concentration range of (a) 0–50 μM and (b) 0–600 μM Na_2SO_3 .

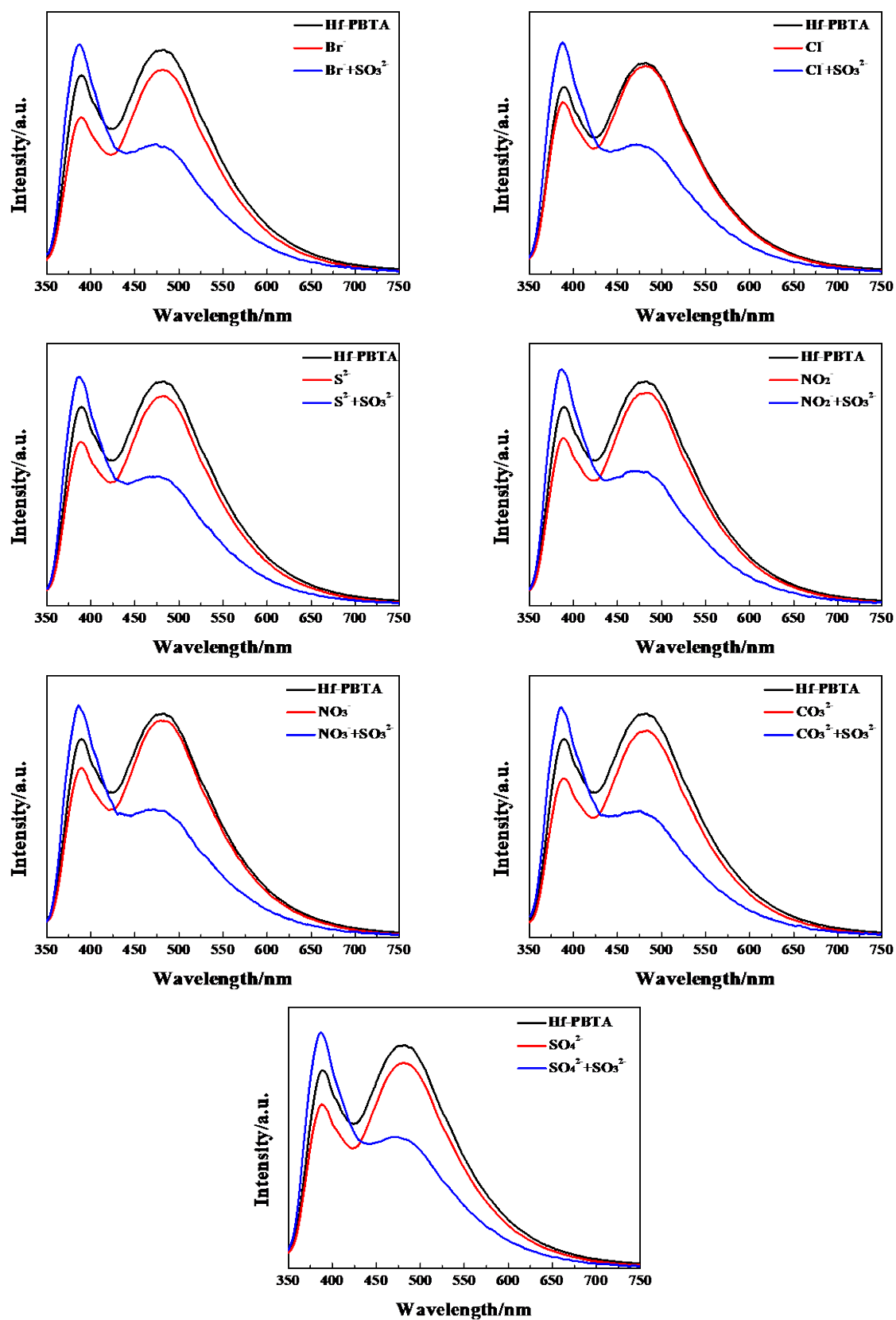


Fig. S28 Competition experiments: Fluorescence spectra of Hf-PBTA before and after adding other anions, and added SO_3^{2-} to the above solution (Ex = 330 nm).

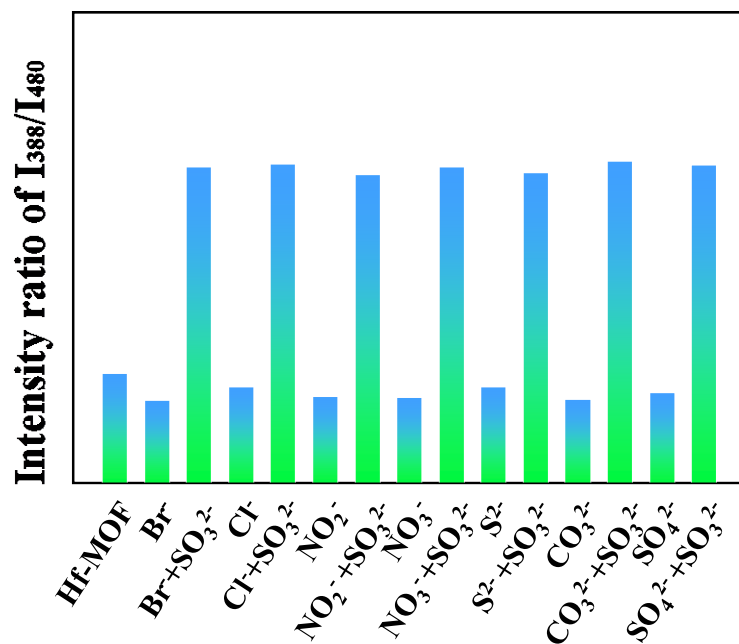


Fig. S29 Anti-interference ability of Hf-PBTA for fluorescent sensing SO_3^{2-} .

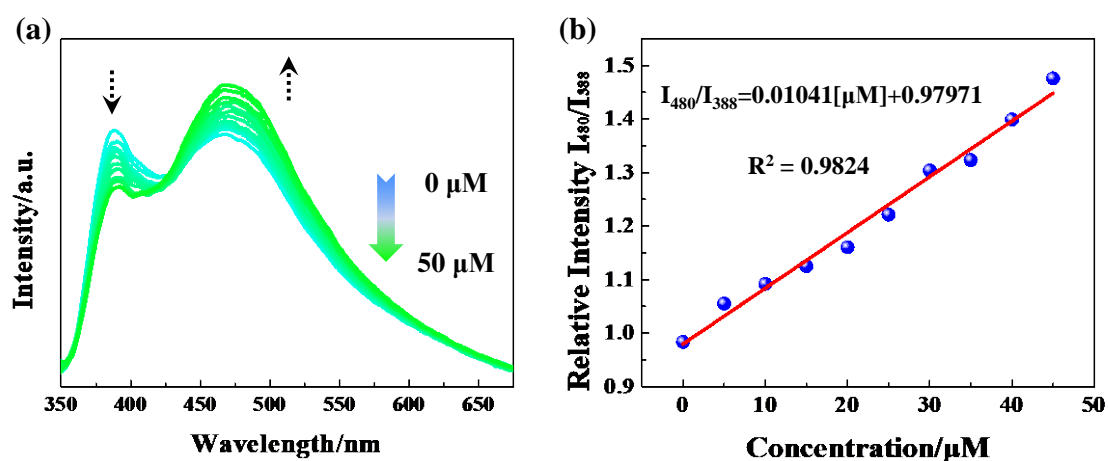


Fig. S30 (a) Effect on the fluorescence of Hf-PBTA dispersed in water upon the incremental addition of SMA (Ex = 330 nm); (b) linear fit for the estimation of detection limit.

Table S1. Literature survey of the H₄PBTA based MOFs.

No.	MOF	Dimension	Property	References
1	PCN-333-Fe(III)	3D	Stability	<i>Angew. Chem. Int. Ed.</i> 2017, 56, 6478
2	PCN-333-Cr(III)	3D	Stability	<i>Angew. Chem. Int. Ed.</i> 2017, 56, 6478
3	[Zr ₆ O ₄ (OH) ₈ (H ₂ O) ₄ (L ²) ₂] (BUT-15)	3D	<u>Fluorescent sensor</u> (Fe ³⁺ ions sensing)	<i>ACS Appl. Mater. Interfaces</i> 2017, 9, 10286
4	Cu ₂ (pbpta)	3D	Gas Adsorption & Catalysis	<i>Cryst. Growth Des.</i> 2017, 17, 2711
5	[Zr ₆ (μ ₃ -O) ₄ (μ ₃ -OH) ₄ (OH) ₄ (L) ₂ -(H ₄ L) _{0.7}] (MFM-600)	3D	SO ₂ adsorption	<i>J. Am. Chem. Soc.</i> 2018, 140, 15564
6	[Zr ₆ (μ ₃ -O) ₄ (μ ₃ -OH) ₄ (OH) ₄ (H ₂ O) ₄ (L) ₂] (MFM-601)	3D	SO ₂ adsorption	<i>J. Am. Chem. Soc.</i> 2018, 140, 15564
7	[(CH ₃) ₂ NH ₂][In(L)]·2.5DMF·2H ₂ O (FJU-16)	3D 4-fold interpenetrated	Proton Conductivity	<i>Cryst. Growth Des.</i> 2018, 18, 3724
8	[(CH ₃) ₂ NH ₂][In(L)]·4.5DMF·16H ₂ O (FJU-17)	3D 2-fold interpenetrated	Proton Conductivity	<i>Cryst. Growth Des.</i> 2018, 18, 3724
9	{[NH ₂ (CH ₃) ₂][In(L)]·2DMF·H ₂ O} (V103)	3D	Catalysis	<i>Inorg. Chem. Front.</i> , 2018, 5, 1694
10	[In(PBPTTBA)][(CH ₃) ₂ NH ₂] (BUT-29)	3D	Dye absorption	<i>Chinese Chemical Letters</i> 2019, 30 234
11	{[In ₃ OL _{1.5} (H ₂ O) ₃](NO ₃) ₃ ·(DMA) ₃ ·(CH ₃ CN) ₆ ·(H ₂ O) ₃₀ } _n (FJU-10)	3D	Proton conduction & <u>Fluorescent sensor</u> (aniline sensing)	<i>ACS Appl. Mater. Interfaces</i> 2019, 11, 16490
12	{[Eu(PPTA) _{0.5} (NO ₃)(DMF) ₂ ·H ₂ O]} _n (V104)	3D	<u>Fluorescent sensor</u> (pH sensing)	<i>Anal. Chem.</i> 2019, 91, 5455–5460

Table S2. The limit of detection of selected analytes.

Analytes	The limit of detection (LOD)	Linear range	Correlation Coefficients (R ²)
Benzenesulfonic acid (BSA)	0.192 ppm	0-50 μM	0.9823
p-Toluenesulfonic acid (TSA)	0.175 ppm	0-50 μM	0.9904
Pyridine-3-sulfonic acid (PSA)	0.181 ppm	0-20 μM	0.9824
SO ₃ ²⁻	0.076 ppm	0-50 μM	0.9927
Sulfamethazine (SMA)	0.688 ppm	0-45 μM	0.9824

References

- 1 Accelrys, Inc., Materials Studio, 4.3V, Accelrys, Inc., San Diego, CA, 2008.
- 2 A. K. Rappe, C. J. Casewit, K. S. Colwell, K. S. Colwell, W. A. GoddardIII and W. M. Skiff, *J. Am. Chem. Soc.*, 1992, **114**, 10024-10035.
- 3 D. A. Gomez-Gualdron, O. V. Gutov, V. Krungleviciute, B. Borah, J. E. Mondloch, J. T. Hupp, T. Yildirim, O. K. Farha and R. Q. Snurr, *Chem. Mater.*, 2014, **26**, 5632-5639.
- 4 M. H. Beyzavi, R. C. Klet, S. Tussupbayev, J. Borycz, N. A. Vermeulen, C. J. Cramer, J. F. Stoddart, J. T. Hupp and O. K. Farha, *J. Am. Chem. Soc.*, 2014, **136**, 15861-15864.
- 5 P. Deria, D. A. Gomez-Gualdron, W. Bury, H. T. Schaefer, T. C. Wang, P. K. Thallapally, A. A. Sarjeant, R. Q. Snurr, J. T. Hupp and O. K. Farha, *J. Am. Chem. Soc.*, 2015, **137**, 13183-13190.
- 6 T. C. Wang, W. Bury, D. A. Gomez-Gualdron, N. A. Vermeulen, J. E. Mondloch, P. Deria, K. Zhang, P. Z. Moghadam, A. A. Sarjeant, R. Q. Snurr, J. F. Stoddart, J. T. Hupp and O. K. Farha, *J. Am. Chem. Soc.*, 2015, **137**, 3585-3591.